Detection of Magnetic Force Fields at Macroscopic Distances with a Micromechanical Cantilever Oscillator

C Iacovita, M Vomir, B Donnio, J L Gallani, M V Rastei

Detection of Magnetic Force Fields at Macroscopic Distances with a Micromechanical Cantilever Oscillator

C. Iacovita[1,2], M. Vomir[1], B. Donnio[1], J.L. Gallani[1], M.V. Rastei*[1]

[1] *Institut de Physique et Chimie des Matériaux de Strasbourg, CNRS, Université de Strasbourg, F-67034 Strasbourg, France*

[2] *Department of Pharmaceutical Physics-Biophysics, Faculty of Pharmacy, "Iuliu Hatieganu" University of Medicine and Pharmacy, 400349 Cluj-Napoca, Romania*

Abstract: We report a procedure for measuremingt magnetic field gradients generated by a macroscopic coil. A micromechanical cantilever oscillator covered with a magnetic material is used to detect variations of the magnetic force field at distances exceeding several times the coil diameter (4 mm). The detection is based on the phase of the first eigenmode of the cantilever while modulating the magnetic field at low frequencies. The nanoscale oscillation of the cantilever along with the high-quality resonance factor are responsible for a coherent oscillation allowing high sensitivity. A detection sensitivity, under ambient conditions, of the order of 10^{-13} T/nm^2 is estimated with the help of numerical calculations. The approach is useful for measuring the spatial variation of the magnetic field gradients generated by any source of magnetic field when the magnetic field can be modified at rates below the resonant frequency of the cantilever. These results can be useful for gradient fields monitoring in macro- and micro-scale magnetic resonance imaging, non-contact electric currents identification from stray magnetic fields, electrical power monitoring, 3D-magnetic fields mapping, or miniature orientation devices.

Keywords: Magnetic stray fields, sensing, micro-cantilever phase dynamics, magnetic forces

I. INTRODUCTION

High-resolution sensing of magnetic field gradients[1] is essential for various applications including nuclear and electron magnetic resonance[2,3], electric micro/macro motors[4,5,6], translational medicine[7,8], or biophysics[9,10,11]. Magnetic fields can be generated by a variety of electric and magnetic components such as permanent magnets[12,13], electrical coils[14,15,16], and transformers[17,18], or generically, by any electric power line or charge-carrier currents[19,20]. They are of growing concern in hybrid and electric vehicles[21], medical instrumentation[22], quantum information technologies[23], and other domains where interaction fields controls or impacts the operation of electric and magnetic components. The evaluation of the spatial variation of the field outside a magnetic field source is therefore of paramount importance. Nevertheless, the measurement of a field gradient is complexified as the distance from the field source is large and a high spatial resolution is required[24].

There are several techniques able to measure magnetic fields[25,26,27], with the most recurrent and sensitive being based on low-temperature SQUIDs[28]. This technique has a high sensitivity but it has the disadvantage of not being a spatially-resolved method. Alternatively, solid-state sensors which include magneto-diodes, magneto-transistors, Hall-effect devices or magneto-resistors have been considered[29,30]. To achieve even higher spatial resolutions, methods based on optical detection of spin properties in scanning probe tips presenting well defined atomic defects, such as nitrogen vacancies in diamond, have been recently developed[31,32,33]. While these methods have indeed demonstrated high spatial resolution in the measurement of magnetic fields, they are not suited for magnetic field gradient detections[34,35,36,37] or for a direct evaluation of the spatial variation of the magnetic field gradients.

Magnetic force microscopy (MFM)[38,39,40] is known as a tool for visualizing the stray field distribution above magnetic nanostructures of dimensions down to individual nanoparticles[41,42]. MFM uses the magnetic interactions between the magnetic probe and the magnetic stray field emerging from the sample.

The signal is generally measured by converting the magnetic interaction into the amplitude or phase change of a cantilevered magnetic tip, yielding a force *gradient* mapping[38], which is a measure of the variation of the magnetic field gradient.

In the present work, we present a method, based on a MFM set-up, able to measure, with nanometer scale resolution, *spatial variations of the gradient* of the magnetic field at macroscopic distances from the magnetic field source. The method is particularly adapted for measuring dynamic fields such as those generated by variable currents or micro/macro coils powered with currents presenting low-frequency components. In addition, the results can be of interest for direct excitation methods of micromechanical cantilevers, where a driving force is directly applied to the cantilever without acoustic transmission through additional components, methods particularly valuable when operating in liquids. Along with photothermal driving[43,44], magnetic excitations of cantilevers are indeed possible by attaching a magnetic bead to the cantilever[45,46,47] or by coating the cantilever with a magnetic thin film[48].

II. EXPERIMENTAL DETAILS

Experiments were performed using an atomic force microscope (AFM) apparatus operating at ambient conditions. The microscope was adapted to allow acquisition of phase signals without a nearby surface, such that the cantilever remains free to oscillate without any interactions other than those induced by the magnetic field gradient. The probes were silicon cantilevers covered with a hard-magnetic coating presenting a coercive field of about 300 Oe and a remnant magnetization of about 300 emu/cm^3 (NanoSensors^{TM} – code: PPP-MFMR). The spring constant of the cantilever was k = 2.8 N/m and the resonance quality factor Q = 660, resulting in a Q/k ratio of 235. The resonance frequency of the cantilever is about 75 kHz. The amplitude of the cantilever oscillations was set to a few tens of nm. An iron core coil was employed to generate the magnetic field. An AC current of rectangular shape with a frequency

of 1 Hz was supplied to the coil, generating an alternating magnetic field around the coil. The cantilever was continuously excited at resonance with the help of a piezoelectric element placed in contact with the cantilever support. The phase of the excitation was continuously compared with the oscillation phase of the cantilever which was monitored with the help of the optical detection system of the AFM microscope. The optical system consisted in a standard deflection system composed of a laser beam (670 nm) and a four-quadrant photodiode.

III. EXPERIMENTAL RESULTS

The oscillation phase of the cantilever was tracked using a lock-in amplifier. This gives a phase shift ($\Delta\phi$) signal which is evaluated by comparing the cantilever phase with respect to the mechanical excitation phase. A schematic of the detection configuration is shown in Fig. 1 (a). The current intensity through the coil was chosen low enough to produce magnetic fields with strengths below the coercive field of the magnetic coating. As a consequence, the magnetization of the cantilever coating remained constant and fixed along the cantilever axis (horizontal ***x***-axis).

A. Phase signal formation and detection

Figure 1 (b) shows an example of the phase shift of the cantilever as a function of time for two lateral "***x***" distances with respect to the center of the coil. The vertical position of the cantilever was kept fixed at ***z*** = 0.6 mm with respect to the surface of the coil end. It can be seen that the phase signal presents abrupt changes of sign at a rate of 1 Hz, indicating a change of the magnetic interaction sign, i.e. from repulsive ($\Delta\phi > 0$) to attractive ($\Delta\phi < 0$). Considering the magnetic interaction component along the oscillation direction of the cantilever (***z***-axis) the phase shift can be written as:[38,49]

$$\Delta\phi = -\frac{Q}{k}\frac{dF_z}{dz} \qquad (1)$$

with Q the quality factor of the cantilever, k the spring constant, and $\frac{dF}{dz}$ the gradient of the magnetic

force along the ***z***-axis. The ratio Q/k is therefore critical for the phase signal sensitivity. Accordingly, $\Delta\phi$ signal is similar to the phase measurements used in MFM with the difference that, in the present case, the relevant magnetization is that of the cantilever coating which is along the ***x***-axis (horizontal). This magnetization interacts with the ***x***-component of the magnetic field (H_x). The interaction is not constant along the ***z***-axis, because H_x varies with ***z***, giving rise to an interaction gradient along ***z***, *i.e.* a force F_z. Since the cantilever oscillates along the ***z***-direction (vertical), only force gradients along ***z***-axis can change the oscillation phase. The force gradient is thus given by the interaction between the magnetization of the cantilever [M_c – blue arrow in Fig. 1(a), which is fixed], and H_x generated by the coil, which moreover changes direction [red arrow in Fig. 1(a)]. Nonetheless, in each case, (insets with antiparallel/parallel arrows) the cantilever senses a force gradient when oscillating up and down. This is given by the second derivative of H_x along the ***z***-axis:

$$\frac{dF_z}{dz} = \int_V M_c \frac{\partial^2 H_x}{\partial z^2} dV \,, \qquad (2)$$

where the integral is over the whole magnetic volume of the cantilever.

It is therefore important to stress that the magnetic interaction is along the ***x***-axis. Because of the cantilever vibration axis $\Delta\phi$ detects the gradient of the respective force along ***z***-axis (see below for details). According to Eq. 1, positive and negative values of $\Delta\phi$ indicate changes in the magnetic interaction sign, which follows the inversion of the current direction within the coil. In Fig. 1, the positive and negative values of $\Delta\phi$ are symmetrical with respect to zero because of the inversion of the current into the coil. More importantly, the magnitude of $\Delta\phi$ depends on the position of the cantilever with respect to the center of the coil (Fig. 1). For instance, in Fig. 1, it is shown that a large $\Delta\phi$ value is recorded when the cantilever is placed at 1.8 mm on the ***x***-axis, whereas the signal drops considerably at 11.3 mm. Nonetheless, it is remarkable to have a detectable signal at such large distances from the coil. Note that for a constant

cantilever magnetization, the value of $\Delta\phi$ is proportional to the variation of the magnetic field gradient generated by the coil at the cantilever position.

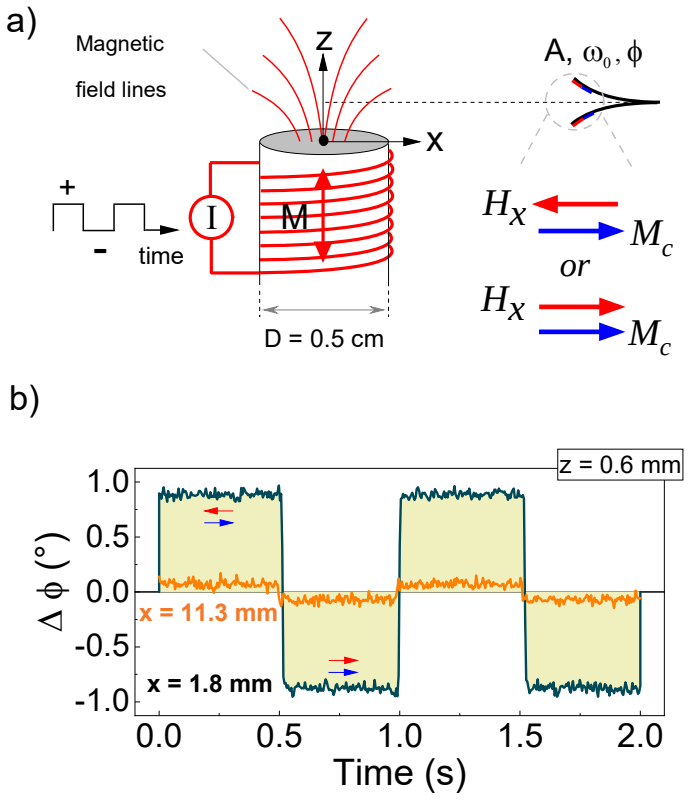

Fig. 1. (a) Schematic of magnetic field generated by a coil as probed with a micromechanical cantilever system. The (0,0) origin of the (***x***, ***y***) axes is located at the center of the coil end (black dot). All **x** and ***z*** values in the manuscript refer to locations of the cantilever with respect to this (0,0) position. (b) Phase shift signal for two periods of magnetic stray field modulated at f = 1 Hz recorded at two different locations on the ***x***-axis and a vertical distance of ***z*** = 0.6 mm.

Our set-up enables the detection of the variation of magnetic field gradients at any positions around the coil. As a second example, we show the results with the cantilever at ***z*** = 1 mm and different locations along the ***x***-axis. The phase shift, recorded over two periods of alternating magnetic field, is shown in Fig.

2. In the first interval 0 – 2.4 mm, the absolute value of $\Delta\phi$ increases as the cantilever approaches the coil edge [Fig. 2 (a)]. Then, between 3.0 – 20.3 mm, $\Delta\phi$ progressively decreases closer to zero [Fig. 2 (b)].

In Fig. 3, the mean values of $\Delta\phi$ as a function of $\boldsymbol{x}$-displacement for both attractive and repulsive magnetic interaction regimes are shown. There is a symmetrical distribution of the $\Delta\phi$ signal when comparing the two regimes, which is due to the symmetric but opposite current flows into the coil at the frequency of 1 Hz.

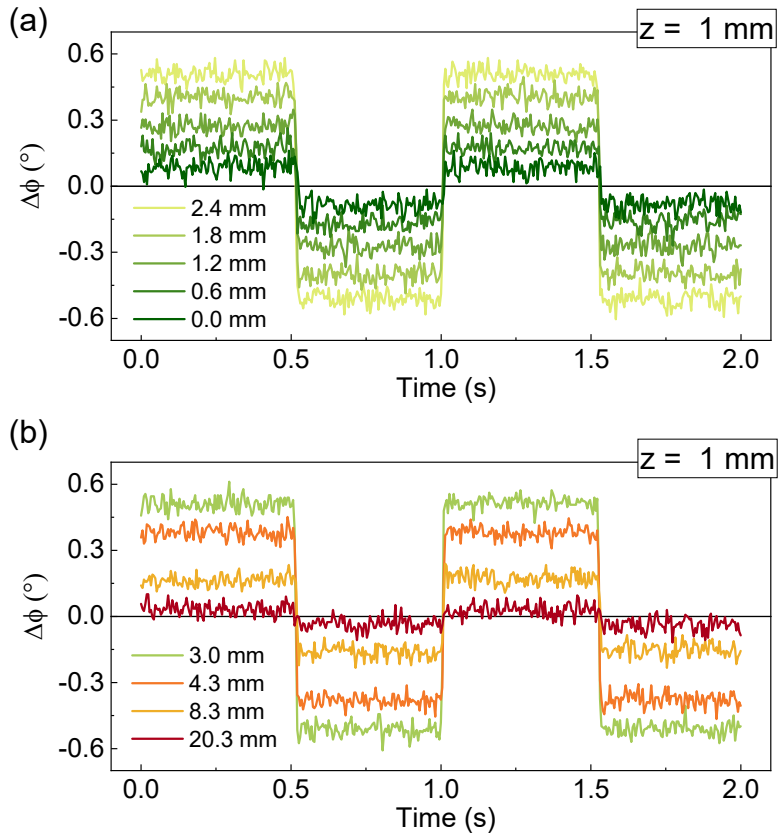

Fig. 2. Phase shift $\Delta\phi$ signal at $\boldsymbol{z}$ = 1 mm for $\boldsymbol{x}$ = 0.0 – 2.4 mm interval (a), and $\boldsymbol{x}$ = 3.0 – 20.3 mm interval (b), respectively. The data is traced as a function of time for two periods of alternating magnetic field (f = 1 Hz). Note that the signal progressively increases in (a) as the cantilever approaches 2.4 mm, i.e. the edge of the coil, then the signal decreases when the cantilever is getting further away from the coil (b).

The evolution of the $\Delta\phi$ signal along $\boldsymbol{x}$ displays the same trend at several lifts, although as can be seen, the magnitude of the signal is larger for $\boldsymbol{z}$ = 0.6 mm than for $\boldsymbol{z}$ = 1.0 mm, as the cantilever is closer to the coil. A maximum signal is measured at about $\boldsymbol{x}$ = 2.6 mm and $\boldsymbol{x}$ = 2.4 mm for $\boldsymbol{z}$ = 1.0 mm and $\boldsymbol{z}$ = 0.6 mm, respectively. The fact that the phase signal presents a maximum at these values indicates that the field gradient of $\boldsymbol{H_x}$ (second derivative of $\boldsymbol{H_x}$ with respect to $\boldsymbol{z}$) is maximum at $\boldsymbol{x}$-distances comparable with the radius of our coil, *i.e.* at the coil edges (see Fig.1). For a magnetization direction inside the coil aligned along the $\boldsymbol{z}$-direction, the $\boldsymbol{x}$-components of the magnetic stray field are indeed expected to be maximum above the coil edges, providing that the measurements are performed at modest lifts (i.e. $\boldsymbol{z}$-values).

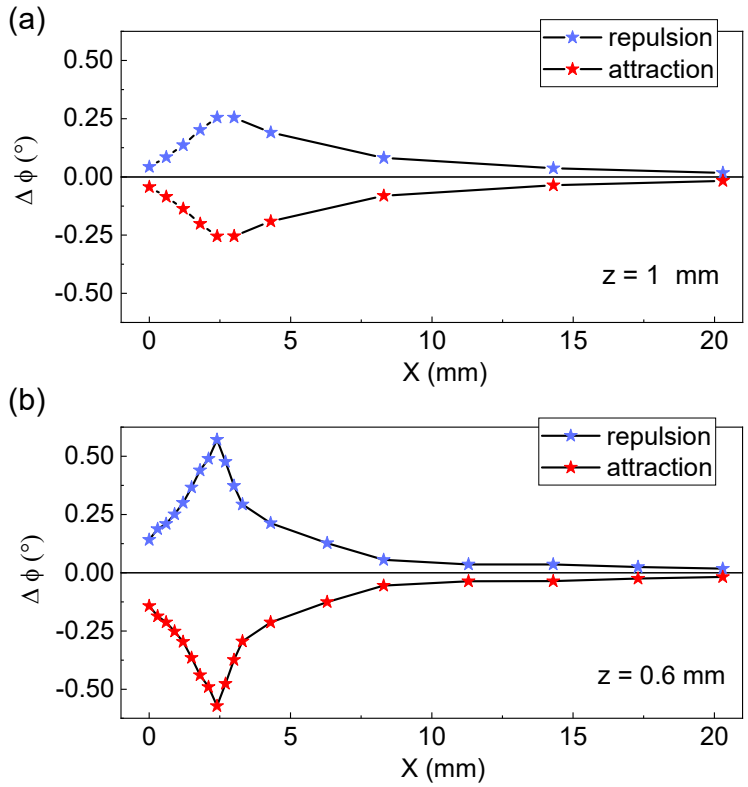

Fig. 3. Phase shift $\Delta\phi$ signal as a function of the lateral position of the cantilever (along the $\boldsymbol{x}$ axis) for $\boldsymbol{z}$ = 1.0 mm (a), and $\boldsymbol{z}$ = 0.6 mm (b) for both interaction regimes – repulsion and attraction. The maximum of the signal at about 2.5 mm corresponds to the edge of the coil, where the $\boldsymbol{H_x}$ magnetic field is indeed expected large.

To give an estimation for the detection limit of our technique, we calculate the $\boldsymbol{H_x}$ magnetic field generated by a magnetized iron cylinder using the analytical expressions from Caciagli et al.[50]. The numerical results are shown in Fig. 4. The strength of the $\boldsymbol{H_x}$ magnetic field generated above the upper base (top) of the iron cylinder is presented in Fig. 4 (a). The (0,0) coordinates represents the center of the upper base of the cylinder (also see Fig. 1). In Fig. 4 (a), it can be seen that the $\boldsymbol{H_x}$ magnetic field is rather weak (red color) with the exception of a region near the edge of the cylinder, where the field presents a maximum (blue color). The field value of this maximum decays along the ***z***-axis, as expected (see color scale).

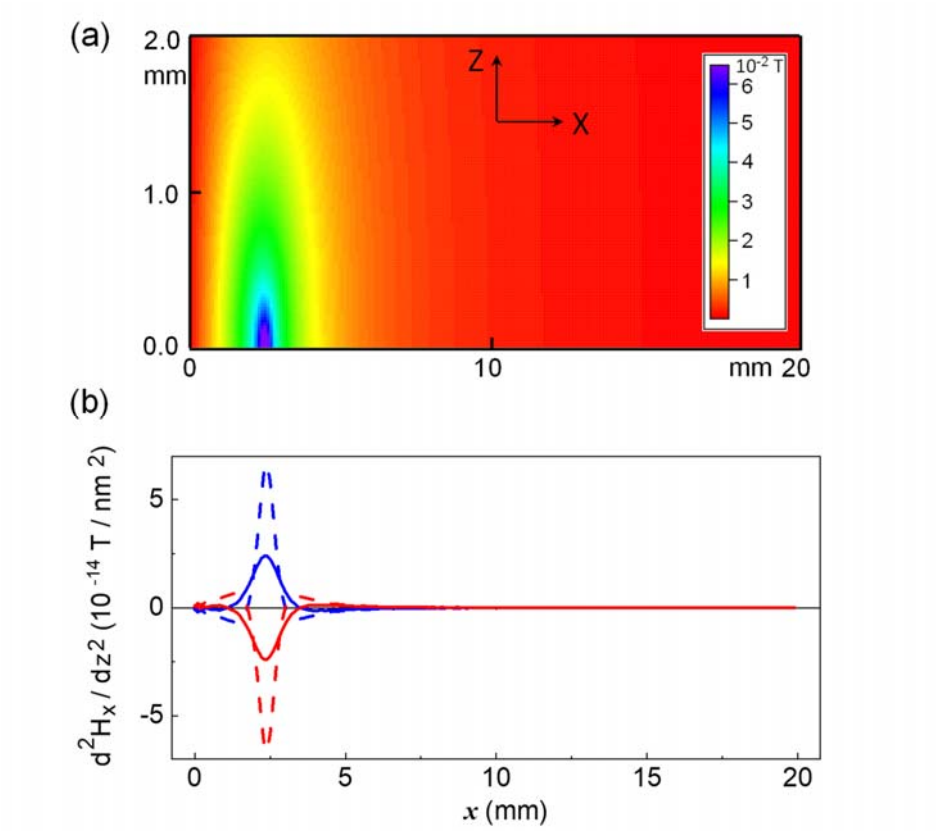

Fig. 4. (a) Calculated two-dimensional map of the ***x***-component of the magnetic field ($\boldsymbol{H_x}$) in the **z-x** plane. (b) Second derivative of the $\boldsymbol{H_x}$ with respect to **z**, calculated at z = 0.6 mm (dashed) and z = 1.0 mm (solid). Blue and red colors correspond to right and left orientations of the field, which is given by up and down magnetized cylinder, respectively.

The calculated fields from Fig. 4 (a) permit the calculation of the first and second derivative of $\boldsymbol{H_x}$ with respect to $\boldsymbol{z}$, at any $\boldsymbol{z}$ distance. The variation of the second derivative of $\boldsymbol{H_x}$ with respect to $\boldsymbol{z}$ ($d^2\boldsymbol{H_x}/d\boldsymbol{z}^2$) along the $\boldsymbol{x}$-axis, at $\boldsymbol{z}$ = 0.6 mm (dashed curves) and $\boldsymbol{z}$ = 1.0 mm (solid curves) is shown in Fig. 4 (b). As expected, the shape of the peaks does not perfectly reproduce the experimental data, because the experimental coil is not a perfect cylinder.. Nevertheless, the maximum values of $d^2\boldsymbol{H_x}/d\boldsymbol{z}^2$ at about 2.5 mm clearly show the dominant role played by the $\boldsymbol{x}$-components of the magnetic field, as well as their spatial variations. These calculations agree with the phase measurements and show that the second derivative of the $\boldsymbol{H_x}$ is indeed responsible for the configuration of the phase variation along the $\boldsymbol{x}$-direction. The values of $d^2\boldsymbol{H_x}/d\boldsymbol{z}^2$ are of the order of 10^{-14} T/nm^2, presenting a maximum at about $\boldsymbol{x} = \boldsymbol{R}$ = 2.5 mm. This agrees with the experimental $\Delta\phi$ signal from Fig. 3. Thus, it can be concluded that spatial variations of the gradients of the magnetic field of the order of 10^{-13} T/nm^2 can readily be detected. Note that this estimation of the detection limit, which is almost one order of magnitude below the calculation values, is not given directly by the experiments but rather by the comparison with the numerical data.

VI. CONCLUSION

In conclusion, the oscillation phase of a micromechanical cantilever covered with a magnetic thin film can be used to measure spatial variations of the magnetic field generated by an electromagnet at centimetric distances. The technique can be useful for mapping magnetic field homogeneities of electromagnetic devices or for detecting embedded magnetic objects in non-magnetic materials. The experiments realized in the present study at *cm*-scale distances can in principle be applied to detect variations of the magnetic fields generated by a large variety of field sources, providing that the field can be periodically varied at low frequencies.

Notes

The authors declare no competing financial interest.

VIII. ACKNOWLEDGEMENTS

We thank N. Beyer for technical assistance. This work is supported by ANR OH-RISQUE SMARAGD (14 OHRI 0008 01). C. Iacovita acknowledges financial support from the Romanian Ministry of Education and Research, CNCS - UEFISCDI, through research project number PN-III-P1-1.1-TE-2019-1392, within PNCDI III.

IX. REFERENCES :

(1) Niekiel, F.; Su, J.; Bodduluri, M. T.; Lisec, T.; Blohm, L.; Pieper, I.; Wagner, B.; Lofink, F. Highly Sensitive MEMS Magnetic Field Sensors with Integrated Powder-Based Permanent Magnets. *Sensors Actuators A Phys.* **2019**, *297*, 111560. https://doi.org/10.1016/J.SNA.2019.111560.

(2) Stejskal, E. O.; Tanner, J. E. Spin Diffusion Measurements: Spin Echoes in the Presence of a Time-Dependent Field Gradient. *J. Chem. Phys.* **1965**, *42* (1), 288–292. https://doi.org/10.1063/1.1695690.

(3) Kneubühl, F. K. Line Shapes of Electron Paramagnetic Resonance Signals Produced by Powders, Glasses, and Viscous Liquids. *J. Chem. Phys.* **1960**, *33* (4), 1074–1078. https://doi.org/10.1063/1.1731336.

(4) Barbic, M.; Mock, J. J.; Gray, A. P.; Schultz, S. Electromagnetic Micromotor for Microfluidics Applications. *Appl. Phys. Lett.* **2001**, *79* (9), 1399–1401. https://doi.org/10.1063/1.1398319.

(5) Wagner, B.; Kreutzer, M.; Benecke, W. Permanent Magnet Micromotors on Silicon Substrates. *J. Microelectromechanical Syst.* **1993**, *2* (1), 23–29. https://doi.org/10.1109/84.232591.

(6) Baraban, L.; Makarov, D.; Schmidt, O. G.; Cuniberti, G.; Leiderer, P.; Erbe, A. Control over Janus Micromotors by the Strength of a Magnetic Field. *Nanoscale* **2013**, *5* (4), 1332–1336. https://doi.org/10.1039/c2nr32662k.

(7) Melville, D.; Paul, F.; Roath, S. High Gradient Magnetic Separation of Red Cells from Whole Blood. *IEEE Trans. Magn.* **1975**, *11* (6), 1701–1704. https://doi.org/10.1109/TMAG.1975.1058970.

(8) Arruebo, M.; Fernández-Pacheco, R.; Ibarra, M. R.; Santamaría, J. Magnetic Nanoparticles for Drug Delivery. *Nano Today* **2007**, *2* (3), 22–32. https://doi.org/10.1016/S1748-0132(07)70084-1.

(9) Ferrari, M. Cancer Nanotechnology: Opportunities and Challenges. *Nature Reviews Cancer*. March 2005,

pp 161–171. https://doi.org/10.1038/nrc1566.

(10) Kilinc, D.; Lee, G. U. Advances in Magnetic Tweezers for Single Molecule and Cell Biophysics. *Integr. Biol.* **2014**, *6* (1), 27–34. https://doi.org/10.1039/c3ib40185e.

(11) He, X.; Yablonskiy, D. A. Biophysical Mechanisms of Phase Contrast in Gradient Echo MRI. *Proc. Natl. Acad. Sci. U. S. A.* **2009**, *106* (32), 13558–13563. https://doi.org/10.1073/pnas.0904899106.

(12) Bloom, A. L.; Packard, M. E. Magnets and Magnetic Field Measurements. *Science*. American Association for the Advancement of Science pp 738–741. https://doi.org/10.2307/1751852.

(13) Coey, J. M. D. Permanent Magnet Applications. *Journal of Magnetism and Magnetic Materials*. Elsevier 2002, pp 441–456. https://doi.org/10.1016/S0304-8853(02)00335-9.

(14) Herlach, F.; McBroom, R. Megagauss Fields in Single Turn Coils. *J. Phys. E.* **1973**, *6* (7), 652–654. https://doi.org/10.1088/0022-3735/6/7/020.

(15) Golay, M. J. E. Field Homogenizing Coils for Nuclear Spin Resonance Instrumentation. *Rev. Sci. Instrum.* **1958**, *29* (4), 313–315. https://doi.org/10.1063/1.1716184.

(16) Autler, S. H. Superconducting Electromagnets. *Rev. Sci. Instrum.* **1960**, *31* (4), 369–373. https://doi.org/10.1063/1.1716985.

(17) Ilonen, K.; Markkanen, A.; Mezei, G.; Juutilainen, J. Indoor Transformer Stations as Predictors of Residential ELF Magnetic Field Exposure. *Bioelectromagnetics* **2008**, *29* (3), 213–218. https://doi.org/10.1002/bem.20385.

(18) Jackman, R. J.; Rogers, J. A.; Whitesides, G. M. Fabrication and Characterization of a Concentric Cylindrical Microtransformer. *IEEE Trans. Magn.* **1997**, *33* (4), 2501–2503. https://doi.org/10.1109/20.595907.

(19) Canova, A.; Giaccone, L.; Lavecchia, G.; Ribaldone, P. Passive Mitigation of Stray Magnetic Fields Generated by Underground Power Lines. In *Conference Proceedings - 2017 17th IEEE International Conference on Environment and Electrical Engineering and 2017 1st IEEE Industrial and Commercial Power Systems Europe, EEEIC / I and CPS Europe 2017*; Institute of Electrical and Electronics Engineers Inc., 2017. https://doi.org/10.1109/EEEIC.2017.7977522.

(20) Suzuki, T.; Fukami, S.; Ishiwata, N.; Yamanouchi, M.; Ikeda, S.; Kasai, N.; Ohno, H. Current-Induced Effective Field in Perpendicularly Magnetized Ta/CoFeB/MgO Wire. *Appl. Phys. Lett.* **2011**, *98* (14), 142505. https://doi.org/10.1063/1.3579155.

(21) Jobava, R. G.; Gheonjian, A. L.; Hippeli, J.; Chiqovani, G.; Karkashadze, D. D.; Bogdanov, F. G.; Khvitia, B.; Bzhalava, A. G. Simulation of Low-Frequency Magnetic Fields in Automotive EMC Problems. *IEEE Trans. Electromagn. Compat.* **2014**, *56* (6), 1420–1430. https://doi.org/10.1109/TEMC.2014.2325134.

(22) Baraban, L.; Streubel, R.; Makarov, D.; Han, L.; Karnaushenko, D.; Schmidt, O. G.; Cuniberti, G. Fuel-Free Locomotion of Janus Motors: Magnetically Induced Thermophoresis. *ACS Nano* **2013**, *7* (2), 1360–

1367. https://doi.org/10.1021/nn305726m.

(23) Spiller, T. P. Quantum Information Technology. *Materials Today*. Elsevier January 1, 2003, pp 30–36. https://doi.org/10.1016/S1369-7021(03)00130-5.

(24) Jaafar, M.; Aljabali, A. A. A.; Berlanga, I.; Mas-Ballesté, R.; Saxena, P.; Warren, S.; Lomonossoff, G. P.; Evans, D. J.; De Pablo, P. J. Structural Insights into Magnetic Clusters Grown inside Virus Capsids. *ACS Appl. Mater. Interfaces* **2014**, *6* (23), 20936–20942. https://doi.org/10.1021/AM505682X/SUPPL_FILE/AM505682X_SI_001.PDF.

(25) Pannetier, M.; Fermon, C.; Le Goff, G.; Simola, J.; Kerr, E. Femtotesla Magnetic Field Measurement with Magnetoresistive Sensors. *Science (80-.).* **2004**, *304* (5677), 1648–1650. https://doi.org/10.1126/science.1096841.

(26) Glenn, D. R.; Bucher, D. B.; Lee, J.; Lukin, M. D.; Park, H.; Walsworth, R. L. High-Resolution Magnetic Resonance Spectroscopy Using a Solid-State Spin Sensor. *Nature* **2018**, *555* (7696), 351–354. https://doi.org/10.1038/nature25781.

(27) Laghi, G.; Dellea, S.; Longoni, A.; Minotti, P.; Tocchio, A.; Zerbini, S.; Langfelder, G. Torsional MEMS Magnetometer Operated Off-Resonance for in-Plane Magnetic Field Detection. *Sensors Actuators A Phys.* **2015**, *229*, 218–226. https://doi.org/10.1016/J.SNA.2015.01.027.

(28) Mathai, A.; Song, D.; Gim, Y.; Wellstood, F. C. High Resolution Magnetic Microscopy Using A Dc Squid. *IEEE Transactions on Applied Superconductivity*. 1993, pp 2609–2612. https://doi.org/10.1109/77.233522.

(29) Reig, C.; Cubells-Beltrán, M. D.; Muñoz, D. R. Magnetic Field Sensors Based on Giant Magnetoresistance (GMR) Technology: Applications in Electrical Current Sensing. *Sensors 2009, Vol. 9, Pages 7919-7942* **2009**, *9* (10), 7919–7942. https://doi.org/10.3390/S91007919.

(30) Kurlyandskaya, G. V.; García-Arribas, A.; Barandiarán, J. M. Advantages of Nonlinear Giant Magnetoimpedance for Sensor Applications. *Sensors Actuators A Phys.* **2003**, *106* (1–3), 234–239. https://doi.org/10.1016/S0924-4247(03)00174-2.

(31) Chernobrod, B. M.; Berman, G. P. Spin Microscope Based on Optically Detected Magnetic Resonance. *J. Appl. Phys.* **2005**, *97* (1), 014903. https://doi.org/10.1063/1.1829373.

(32) Taylor, J. M.; Cappellaro, P.; Childress, L.; Jiang, L.; Budker, D.; Hemmer, P. R.; Yacoby, A.; Walsworth, R.; Lukin, M. D. High-Sensitivity Diamond Magnetometer with Nanoscale Resolution. *Nat. Phys.* **2008**, *4* (10), 810–816. https://doi.org/10.1038/nphys1075.

(33) Maze, J. R.; Stanwix, P. L.; Hodges, J. S.; Hong, S.; Taylor, J. M.; Cappellaro, P.; Jiang, L.; Dutt, M. V. G.; Togan, E.; Zibrov, A. S.; Yacoby, A.; Walsworth, R. L.; Lukin, M. D. Nanoscale Magnetic Sensing with an Individual Electronic Spin in Diamond. *Nature* **2008**, *455* (7213), 644–647. https://doi.org/10.1038/nature07279.

(34) Msaed, A.; Chadebec, O.; Delamare, J. A Simple and Accurate Magnetic Gradient Sensor Configuration Dedicated to Electrical Currents Measurements. *Sens. Lett.* **2009**, *7* (3), 497–502. https://doi.org/10.1166/SL.2009.1096.

(35) Mamishev, A. V.; Short, S. X.; Kao, T. W.; Russell, B. D. Nonintrusive Sensing Techniques for the Discrimination of Energized Electric Cables. *IEEE Trans. Instrum. Meas.* **1996**, *45* (2), 457–461. https://doi.org/10.1109/19.492767.

(36) Leilabady, P. A.; Corke, M.; Sweeney, K. L.; Prater, R. L. Measurement Techniques For Magnetic Field Gradient Detection. *Fiber Opt. Laser Sensors IV* **1987**, *0718*, 120. https://doi.org/10.1117/12.937505.

(37) Dabsch, A.; Rosenberg, C.; Stifter, M.; Keplinger, F. MEMS Cantilever Based Magnetic Field Gradient Sensor. *J. Micromechanics Microengineering* **2017**, *27* (5), 055014. https://doi.org/10.1088/1361-6439/AA654F.

(38) Grütter, P.; Mamin, H. J.; Rugar, D. Magnetic Force Microscopy (MFM); Springer, Berlin, Heidelberg, 1992; pp 151–207. https://doi.org/10.1007/978-3-642-97363-5_5.

(39) Passeri, D.; Angeloni, L.; Reggente, M.; Rossi, M., Magnetic Force Microscopy, I. *Magnetic Characterization Techniques for Nanomaterials*; Kumar, C. S. S. R., Ed.; Springer Berlin Heidelberg: Berlin, Heidelberg, 2017. https://doi.org/10.1007/978-3-662-52780-1.

(40) Kazakova, O.; Puttock, R.; Barton, C.; Corte-León, H.; Jaafar, M.; Neu, V.; Asenjo, A. Frontiers of Magnetic Force Microscopy. *J. Appl. Phys.* **2019**, *125* (6), 060901. https://doi.org/10.1063/1.5050712.

(41) Rastei, M. V.; Meckenstock, R.; Bucher, J. P.; Devaux, E.; Ebbesen, T. Electrochemical Growth of Co Nanodots on Patterned Si Substrates. *Appl. Phys. Lett.* **2004**, *85* (11), 2050–2052. https://doi.org/10.1063/1.1787597.

(42) Iacovita, C.; Hurst, J.; Manfredi, G.; Hervieux, P. A.; Donnio, B.; Gallani, J. L.; Rastei, M. V. Magnetic Force Fields of Isolated Small Nanoparticle Clusters. *Nanoscale* **2020**, *12* (3), 1842–1851. https://doi.org/10.1039/C9NR08634J.

(43) Umeda, N. Scanning Attractive Force Microscope Using Photothermal Vibration. *J. Vac. Sci. Technol. B Microelectron. Nanom. Struct.* **1991**, *9* (2), 1318. https://doi.org/10.1116/1.585187.

(44) Barsella, A.; Hurier, M. A.; Pichois, M. D.; Vomir, M.; Hasan, H.; Mager, L.; Donnio, B.; Gallani, J. L.; Rastei, M. V. Photonic Excitation of a Micromechanical Cantilever in Electrostatic Fields. *Phys. Rev. Lett.* **2020**, *125* (25), 254301. https://doi.org/10.1103/PHYSREVLETT.125.254301/FIGURES/4/MEDIUM.

(45) Jarvis, S. P.; Oral, A.; Weihs, T. P.; Pethica, J. B. A Novel Force Microscope and Point Contact Probe. *Rev. Sci. Instrum.* **1993**, *64* (12), 3515. https://doi.org/10.1063/1.1144276.

(46) Florin, E. L.; Radmacher, M.; Fleck, B.; Gaub, H. E. Atomic Force Microscope with Magnetic Force Modulation. *Rev. Sci. Instrum.* **1998**, *65* (3), 639. https://doi.org/10.1063/1.1145130.

(47) Hirata, K.; Igarashi, T.; Suzuki, K.; Miyazawa, K.; Fukuma, T. Wideband Magnetic Excitation System for

Atomic Force Microscopy Cantilevers with Megahertz-Order Resonance Frequency. *Sci. Reports 2020 101* **2020**, *10* (1), 1–12. https://doi.org/10.1038/s41598-020-65980-4.

(48) Han, W.; Lindsay, S. M.; Jing, T. A Magnetically Driven Oscillating Probe Microscope for Operation in Liquids. *Appl. Phys. Lett.* **1998**, *69* (26), 4111. https://doi.org/10.1063/1.117835.

(49) Rugar, D.; Mamin, H. J.; Guethner, P.; Lambert, S. E.; Stern, J. E.; McFadyen, I.; Yogi, T. Magnetic Force Microscopy: General Principles and Application to Longitudinal Recording Media. *J. Appl. Phys.* **1998**, *68* (3), 1169. https://doi.org/10.1063/1.346713.

(50) Caciagli, A.; Baars, R. J.; Philipse, A. P.; Kuipers, B. W. M. Exact Expression for the Magnetic Field of a Finite Cylinder with Arbitrary Uniform Magnetization. *J. Magn. Magn. Mater.* **2018**, *456*, 423–432. https://doi.org/10.1016/J.JMMM.2018.02.003.